JOURNAL OF GEOPHYSICAL RESEARCH, VOL. 111, F04004, doi:10.1029/2006JF000461, 2006

Amplified erosion above waterfalls and oversteepened bedrock reaches

I. Haviv,[1,3] Y. Enzel,[1] K. X. Whipple,[2] E. Zilberman,[3] J. Stone,[4] A. Matmon,[1] and L. K. Fifield[5]

Received 3 January 2006; revised 19 May 2006; accepted 14 June 2006; published 24 October 2006.

[1] None of the conventional bedrock erosion laws can predict incision immediately upslope of a waterfall lip where the flow is accelerating toward a freefall. Considering the expected increase in flow velocity and shear stress at the lip of a waterfall, we determine erosion amplification at a waterfall lip as $\frac{E_{lip}}{E_{(x=L_a)}} = \left(1 + \frac{0.4}{Fr^2_{(x=La)}}\right)^{3n}$, where $E_{(x=L_a)}$ is the erosion rate at the upstream end of the flow acceleration zone above a waterfall, Fr is the Froude number at this setting, and n ranges between 0.5–1.7. This amplification expression suggests that erosion at the lip could be as much as 2–5 times higher relative to erosion at a normal setting with identical hydraulic geometry. Utilizing this erosion amplification expression in numerical simulations, we demonstrate its impact on reach-scale morphology above waterfalls. Amplified erosion at the lip of a waterfall can trigger the formation of an oversteepened reach whose length is longer than the flow acceleration zone, provided incision wave velocity (V_i) at the upstream edge of the flow acceleration zone is higher than the retreat velocity of the waterfall face. Such an oversteepened reach is expected to be more pronounced when V_i increases with increasing slope. The simulations also suggest that oversteepening can eventually lead to steady state gradients adjacent to a waterfall lip provided V_i decreases with increasing slope. Flow acceleration above waterfalls can thus account, at least partially, for prevalent oversteepened bedrock reaches above waterfalls. Using the cosmogenic isotope Cl-36, we demonstrate that incision wave velocity upstream of a waterfall at the Dead Sea western escarpment is probably high enough for freefall-induced oversteepening to be feasible.

Citation: Haviv, I., Y. Enzel, K. X. Whipple, E. Zilberman, J. Stone, A. Matmon, and L. K. Fifield (2006), Amplified erosion above waterfalls and oversteepened bedrock reaches, *J. Geophys. Res.*, *111*, F04004, doi:10.1029/2006JF000461.

1. Introduction

[2] Waterfalls, hereby used to describe near vertical drops in channel elevation where water is in a freefall condition, are not only very common in steep bedrock channels but may also persist for million of years. Both waterfall retreat and the rate of lowering of a waterfall lip act as a complex boundary condition influencing the evolution of the reach above it. Oversteepened, convex reaches are commonly found above waterfalls across a range of climatic conditions and lithologies within basins with variable drainage areas and possibly reflect the influence of this complex boundary condition. Such reaches were reported in the Blue Mountains of southeast Australia [*Holland*, 1974] and can also be seen above the Niagara Horseshoe Falls (Figure 1 and Table 1). Five surveyed reaches terminating in waterfalls along the Dead Sea western escarpment also exhibit oversteepened, convex profiles (Figure 1 and Table 1). Although oversteepened reaches could form because of reasons which are not waterfall related, the frequency of their occurrence suggests that they might be genetically linked to waterfalls. Moreover, during a flume study of knickpoint retreat in homogenous cohesive material, *Gardner* [1983] observed accelerated erosion associated with oversteepening of the water surface profile upstream of a freefall. Such a flow pattern could probably be held responsible for rapid stripping of the alluvial mantle upstream from knickpoints formed during 1999 Chi-Chi earthquake [*Sklar et al.*, 2005].

[3] In this paper we present a model of the expected amplification of erosion rate at a waterfall lip in response to flow acceleration toward the freefall and examine the interaction between erosion at the lip, retreat of the waterfall face (Figure 2a), and profile evolution upstream of the waterfall using numerical simulations. Our simulations utilize the standard detachment-limited incision model but modify it to account for hydraulic acceleration immediately upstream of a waterfall. The paper does not intend to discuss lateral erosion processes acting on the vertical face itself. In deriving the relations for amplified erosion at the

[1]Institute of Earth Sciences, The Hebrew University of Jerusalem, Givat Ram, Jerusalem, Israel.
[2]Earth, Atmospheric and Planetary Sciences, Massachusetts Institute of Technology, Cambridge, Massachusetts, USA.
[3]Geological Survey of Israel, Jerusalem, Israel.
[4]Quaternary Research Center, University of Washington, Seattle, Washington, USA.
[5]Department of Nuclear Physics, Australian National University, Canberra, Australia.

0148-0227/06/2006JF000461$09.00

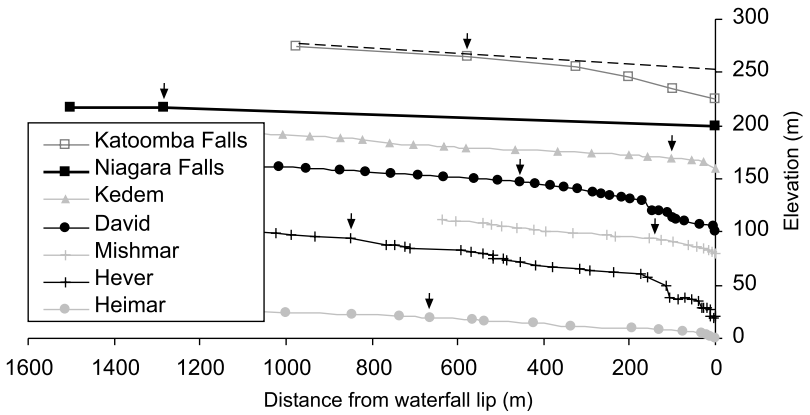

Figure 1. Longitudinal profiles of selected channels showing oversteepened reaches above waterfalls (Table 1). Lowermost five profiles are from channels draining the Dead Sea western escarpment. These profiles were surveyed using a hand level and a laser range finder. Also depicted are the 1300 m long oversteepened reach above the Niagara Horseshoe Falls [modified from *Philbrick*, 1974, Figure 2] and an oversteepened reach above Katoomba Falls in the Blue Mountains, Australia (on the basis of a 1:25,000 map with a 10 m contour interval). None of these reaches cross prominent lithologic boundaries. Dashed black line delineates extrapolation of normal, nonoversteepened gradients toward the lip and is used to define the depth of incision at the lip (Table 1). Arrows mark the upstream end of the oversteepened reach. All the profiles depicted were translated vertically for convenience of presentation. The height of each waterfall is listed in Table 1. The range of waterfall heights is 90–340 m.

lip we first follow and then modify *Stein and Julien* [1993] (on the basis of the work of *Rouse* [1943]) who developed an expression for the time needed to erode a vertical headcut (i.e., step carved in relatively unconsolidated material such as soil) from its lip to its bottom.

2. Erosion of a Waterfall Lip

[4] Conventional erosion laws for bedrock channels treat incision rate as proportional to mean bed shear stress (or unit stream power). By assuming steady uniform flow, these models cast incision rate in terms of channel bed slope as a proxy for water surface slope [e.g., *Howard and Kerby*, 1983; *Whipple and Tucker*, 1999]. Such models cannot capture the influence of flow acceleration and the steepening of the water surface slope immediately upstream of waterfalls. Experimental and theoretical efforts conducted by the hydraulic engineer *Rouse* [1936, 1937, 1943] have demonstrated that water accelerates as it approaches a freefall lip even when the flow is highly supercritical (Froude number value of 3). This seemingly unexpected outcome is the consequence of a pressure gradient force: The flow cross section at the lip is in contact with the air along its lower boundary and often also along its two sides and therefore residual pressures within the lip cross section are expected to be nearly atmospheric rather than hydrostatic (Figure 2).

[5] Assuming conservation of momentum parallel to the channel and neglecting the difference between the driving gravitational force and the resisting friction forces one may write:

$$m_w V_{lip} - m_w V_{(x=L_a)} = \left(P_{(x=L_a)} A_{c(x=L_a)} - P_{lip} A_{c\_lip}\right)\Delta t \qquad (1)$$

where V, P, A_c are average flow velocity parallel to the channel, average cross-sectional hydraulic pressure and

Table 1. Length and Slope Data of Oversteepened Reaches Depicted in Figure 1

Channel Name	Oversteepened Reach Length,[a] m	Slope at the Lip Vicinity	Slope Upstream of the Oversteepened Reach	Depth of Incision at the Lip,[b] m	Waterfall Height, m
Nahal Kedem	100	0.22	0.023	5–10	340
Nahal David	450	0.18	0.029	35	180
Nahal Mishmar	150	0.14	0.033	8–10	160
Nahal Hever	850	0.23	0.031	70	130
Nahal Heimar	660	0.09	0.015	10–20	86
Niagara River[c]	1300	0.015	0.0006	~20	~90[d]
Katoomba Falls[c]	600	0.07	0.025	~25	~140[e]

[a]The upstream edge of each oversteepened reach is marked by an arrow in Figure 1.
[b]The depth of incision at the lip is measured as described in Figure 1.
[c]Channels which are not located along the Dead Sea western escarpment.
[d]The height is relative to the bottom of the Maid of the Mist pool whose depth is ~35–40 m [*Philbrick*, 1970].
[e]On the basis of a 1:25,000 map with a 10 m contour interval.

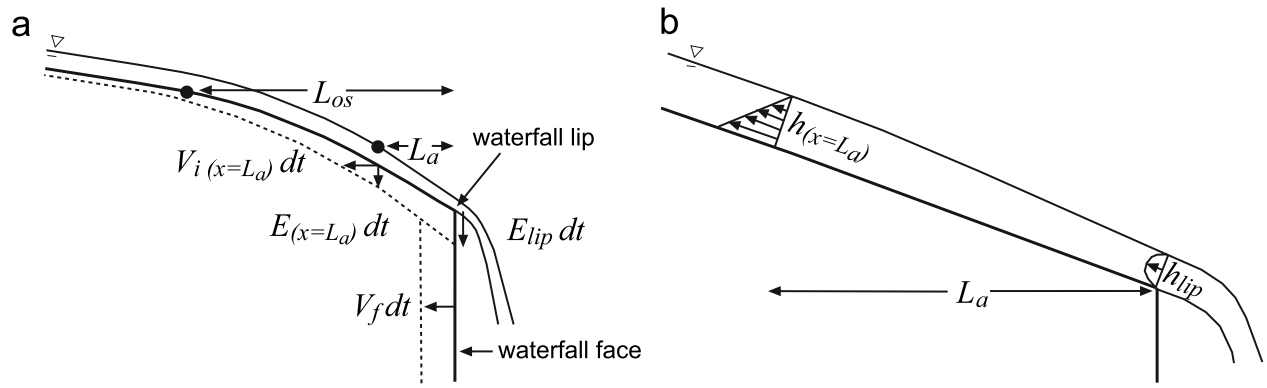

Figure 2. (a) A definition sketch of a waterfall and an oversteepened reach. L_{os} and L_a are the lengths of the oversteepened reach and the hydraulic acceleration zone, respectively. E_{lip} and $E_{(x=L_a)}$ are the erosion rates at the lip and at the upstream edge of the flow acceleration zone. V_f and $V_{i(x=L_a)}$ are waterfall face velocity and incision wave velocity at $x = L_a$. Dashed line depicts channel profile and face location after a time interval, dt. (b) Pressure distribution (arrows) and flow depth (h) at the upper end of the acceleration zone ($x = L_a$) and at the lip cross section. Pressure distribution at $x = L_a$ is hydrostatic. The entire pressure distribution at the lip cross section is close to atmospheric, and therefore a pressure gradient force accelerates the flow between these two cross sections [modified from *Rouse*, 1936].

cross-sectional area, respectively. The subscript *lip* denotes the waterfall lip whereas the subscript $x = L_a$ denotes the upstream edge of the flow acceleration zone at a distance L_a from the lip (Figure 2). m_w is the mass of water entering the acceleration zone and crossing the waterfall lip during time Δt.

[6] Neglecting residual pressure at the lip, and assuming a wide, rectangular cross section, equation (1) can be cast as:

$$\frac{\rho q^2 w \Delta t}{h_{lip}} - \frac{\rho q^2 w \Delta t}{h_{(x=L_a)}} = \frac{1}{2}\rho g h^2_{(x=L_a)} w \Delta t \cos\alpha \tag{2}$$

where ρ is water density, q is discharge per unit width, w is channel width, g is gravitational acceleration, h is flow depth and α is channel slope measured in degrees. Rearranging equation (2) yields:

$$\frac{q^2}{g h_{lip} h^2_{(x=L_a)}} - \frac{q^2}{g h^3_{(x=L_a)}} = \frac{\cos\alpha}{2} \tag{3}$$

The flow Froude number (Fr) at the upstream edge of the acceleration zone can be expressed as:

$$Fr^2_{(x=L_a)} = \frac{q^2}{g h^3_{(x=L_a)}} \tag{4}$$

[7] Substituting equation (4) into equation (3), rearranging and assuming $\cos\alpha \approx 1$ yields [*Rouse*, 1943]:

$$\frac{h_{(x=L_a)}}{h_{lip}} = \frac{V_{lip}}{V_{(x=L_a)}} = \frac{0.5 + Fr^2_{(x=L_a)}}{Fr^2_{(x=L_a)}} \tag{5}$$

Rouse [1943] noted that equation (5) slightly overestimated his experimental observations of $h_{(x=L_a)}/h_{lip}$. His results, as well as results from later studies [*Delleur et al.*, 1956; *Rajaratnam and Muralidhar*, 1968a, 1968b], are better met using the following equation developed by *Hager* [1983, 1984] utilizing both momentum and energy considerations:

$$\frac{h_{(x=L_a)}}{h_{lip}} = \frac{V_{lip}}{V_{(x=L_a)}} = \frac{0.4 + Fr^2_{(x=L_a)}}{Fr^2_{(x=L_a)}} \tag{6}$$

Considering that some residual pressures do remain at the lip cross section and that the friction force along L_a should exceed the gravitational force the velocity ratio described in equation (6) should be taken as an upper limit.

[8] Using equation (6) and assuming that shear stress (τ) varies with the square of velocity and a spatially uniform friction coefficient, *Stein and Julien* [1993] expressed the amplification of shear stress at a freefall lip as:

$$\frac{\tau_{lip}}{\tau_{(x=L_a)}} = \left(1 + \frac{0.4}{Fr^2_{(x=L_a)}}\right)^2 \tag{7}$$

They then assumed that sediment detachment is a function of excess shear stress and used this function to express the time needed to erase a vertical headcut.

[9] Assuming that incision rate is a power law function of the average cross-sectional shear stress we express amplification of erosion at a freefall lip as:

$$\frac{E_{lip}}{E_{(x=L_a)}} = \left(\frac{\tau_{lip}}{\tau_{(x=L_a)}}\right)^a \tag{8}$$

Many factors can influence the relationship between erosion rate and shear stress; a power law is chosen here to allow exploration of a wide range of plausible erosional responses to the hydrodynamic flow acceleration above a waterfall. Since our analysis is restricted to exploring the effect of shear stress amplification on local erosion rate, we find it convenient to cast the problem in terms of the well-known stream power incision model [e.g., *Howard and Kerby*,

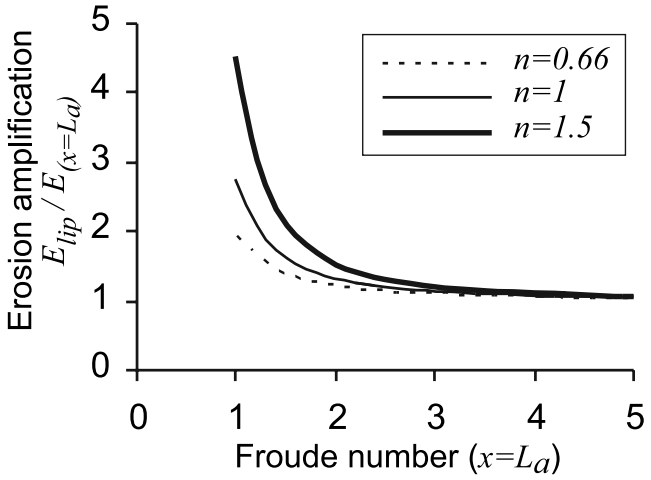

Figure 3. Expected erosion amplification at a waterfall lip as function of the flow Froude number at the upper end of the flow acceleration zone ($Fr_{(x=L_a)}$) and the exponent n.

1983; *Seidl and Dietrich*, 1992; *Rosenbloom and Anderson*, 1994; *Sklar and Dietrich*, 1998; *Whipple and Tucker*, 1999]:

$$E = KA^m S^n \tag{9}$$

where K is erodibility coefficient, A is drainage area, S is channel slope, n is slope exponent and m is drainage area exponent. In this case, the slope exponent n can be written in terms of the shear stress exponent a [*Whipple and Tucker*, 1999]:

$$n = \frac{2}{3}a \tag{10}$$

The range of values reported for n is ~0.5–1.7 [*Stock and Montgomery*, 1999; *Whipple et al.*, 2000]. Note that we explore only the relations among erosion rate, slope, and flow acceleration assuming channel roughness and channel width are constant along L_a.

[10] Combining equations (7), (8), and (10) yields:

$$\frac{E_{lip}}{E_{(x=L_a)}} = \left(1 + \frac{0.4}{Fr^2_{(x=L_a)}}\right)^{3n} \tag{11}$$

Equation (11) expresses the amplification of erosion at a waterfall lip as function of the flow Froude number and the slope exponent n (Figure 3). When $Fr_{(x=L_a)} \approx 1$ erosion at the lip is expected to be ~2–5 times higher than erosion at the upstream edge of the flow acceleration zone. Furthermore, amplification of erosion will occur even when the flow approaching the lip is highly supercritical and will reach insignificant magnitudes only for $Fr_{(x=L_a)} > \sim 3$. For any given Fr erosion amplification increases with n.

3. Model Formulation

[11] An explicit finite difference 1D numerical model is used to examine longitudinal profile evolution above a waterfall lip. Initially, we assume that the vertical face of the modeled waterfall is spatially fixed. Later, we examine the more realistic scenario where the face retreats upstream. The length of the modeled reaches varies from several hundred meters to several kilometers while run time varies from 100 kyr to several Myr. The grid spacing is of submeter scale.

[12] During each time step the model utilizes the Manning equation to calculate the Froude number at the upper end of the acceleration zone. For a wide, rectangular channel this yields:

$$Fr_{(x=L_a)} = \left(\frac{Q}{w}\right)^{0.1} \left(\frac{S^{0.5}_{(x=L_a)}}{n_m}\right)^{0.9} g^{-0.5} \tag{12}$$

where Q is discharge, w is channel width and n_m is Manning roughness coefficient. Discharge per unit width (Q/w) is represented in the model by a power law function of drainage area, which is held invariant over the modeled reaches. Erosion upstream of the flow acceleration zone ($x \geq L_a$) is calculated using the stream power erosion law (equation (9)). Erosion at x = L_a is then used to calculate erosion at the lip as a function of the Froude number at $x = L_a$ and the magnitude of erosion amplification given by equation (11).

[13] Experiments have shown that L_a stretches 2–4 times (r) the depth of the flow at $x = L_a$ [*Rouse*, 1936, 1943; *Rajaratnam and Muralidhar*, 1968a; *Henderson*, 1966]. L_a is calculated in the model using the Manning equation:

$$L_a = rh_{(x=L_a)} = rn_m \left(\frac{Q}{w}\right)^{0.6} S^{-0.3}_{(x=L_a)} \tag{13}$$

This time-dependent variable is represented by a time-dependent spacing between the lip node and the node immediately upstream. This representation assumes that erosion amplification due to the waterfall decays linearly to zero at $x = L_a$.

[14] For all runs discharge is constant along the entire modeled reach and the initial channel profile is linear with a slope of 0.03. Since one of our goals is to isolate and explore the influence of the sensitivity of erosion rate to the shear stress amplification (represented by the slope exponent n), we constrain all runs to have the same initial and background (above the oversteepened zone) erosion rate. For runs with different values of the slope exponent n, this is achieved by adjusting channel erodibility (K).

[15] In simulations where the waterfall face is not fixed its retreat rate, V_f, might be a function of drainage area [*Haviv et al.*, 2003; *Hayakawa and Matsukura*, 2003; *Enzel et al.*, 2005; *Hayakawa et al.*, 2005; *Crosby and Whipple*, 2006]. However, to better understand the interactions between face retreat and incision above the waterfall, we forced a constant retreat rate throughout each simulation, consistent with the assumption of constant drainage area in the reach above the waterfall. The implications of a significant downstream increase in discharge along the modeled reach, which may alter both waterfall retreat velocity and upstream incision, are dealt with in the discussion.

[16] As mentioned earlier, several complexities in natural systems are not explicitly considered in the model: (1) Residual pressures at the lip may actually be roughness

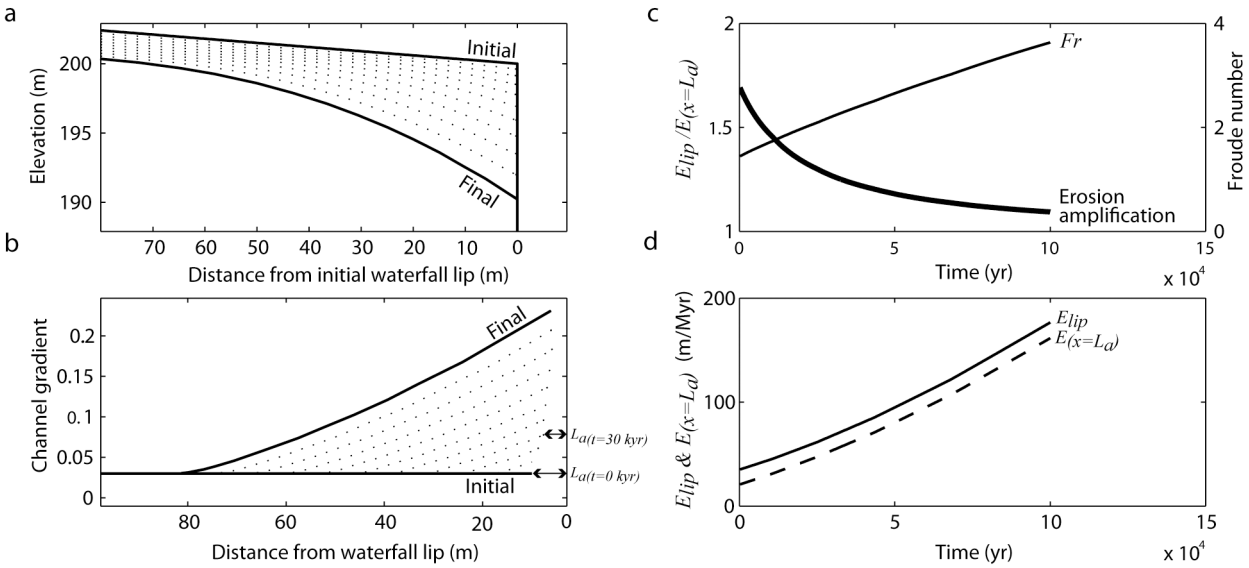

Figure 4. Results of numerical simulation of profile evolution above a waterfall whose face is fixed. Runtime is 100 kyr, and $n = 1$. (a) Initial and final channel profile (solid) and profiles at 10 kyr intervals (dashed). (b) Initial and final channel gradient as a function of the distance from the waterfall lip (solid) and channel gradients at 10 kyr intervals (dashed). Note that L_{os} increases with time reaching 80 m after 100 kyr. L_a decreases from ~10 m to ~6 m. (c) Froude number at the upper end of the acceleration zone (thin line) and erosion amplification (thick line) as function of time. Note that initially, erosion amplification is ~1.7. It decays to ~1.1 within 100 kyr. (d) Erosion rates at the lip (solid) and at $x = L_a$ (dashed) as a function of time.

dependent [*Rajaratnam et al.*, 1976], suggesting that the amplification of velocity, shear stress, and incision at the lip are roughness dependent as well. (2) Both channel roughness and channel width may vary with the distance from the waterfall and with time: Channel width may decrease as the waterfall is approached and thus alter both bed shear stress and the flux of abrasion tools per unit width; this narrowing could increase bed erosion, but may also work in the opposite direction if wall drag is considered [*Johnson and Whipple*, 2004]. (3) Regardless of the bed shear stress, hydraulic plucking at the lip may be more efficient than elsewhere since the freefall edge of blocks at the lip is friction-free [*Hancock et al.*, 1998; *Whipple et al.*, 2000]. (4) Both flow acceleration due to the freefall, and the oversteepening associated with it, will lead to a decrease in the amount of sediment cover on the bed as the lip is approached; this effect could have a profound effect on incision rates since the channel bed will be less armored. Thus the erosional response to freefall-induced flow acceleration must reflect the net effect of several complex influences. Although we could attempt to explicitly model one or more of these effects (e.g., the bed cover effect following *Sklar and Dietrich*, [2004]), we do not yet know how to explicitly determine the integrated effect of all these factors.

4. Model Results

[17] In simulations where the waterfall face is fixed (Figure 4) it loses height as the lip erodes and a convex reach forms upstream (Figure 4a). Channel gradient upstream of the lip increases continuously with time and the convex oversteepened reach lengthens (Figure 4b). As channel gradient increases the Froude number increases and thus the amplification of erosion at the lip decreases (Figure 4c). Despite this decrease in erosion amplification both the erosion rate at $x = L_a$ and the lip erosion rate continue to rise (Figure 4d). If the entire vertical face is eventually consumed the freefall effect will stop and erosion amplification will cease. The remaining break in slope will evolve as predicted by the stream power incision model and discussed elsewhere [e.g., *Whipple and Tucker*, 1999].

[18] In simulations where the waterfall face retreats upstream (Figure 5) an oversteepened reach whose length, L_{os}, is longer than L_a develops only when $V_{i(x=L_a)} > V_f$. Where V_f is the waterfall lateral retreat rate and $V_{i(x=L_a)}$ is the rate at which a point just upstream of the acceleration zone is being translated upstream because of incision. While the term incision rate describes the rate at which a channel point at a given, fixed horizontal location is lowered vertically, V_i describes the rate at which a channel point at a given, fixed elevation is translated horizontally. When measured over a short enough time span this velocity is given by:

$$V_{i(x=L_a)} = \frac{E_{(x=L_a)}}{S_{(x=L_a)}} \tag{14}$$

For cases where the stream power model is adequate to describe incision upstream of $x = L_a$, $V_{i(x,t)}$ is the velocity of a kinematic wave given by [*Rosenbloom and Anderson*, 1994]:

$$V_{i(x,t)} = KA^m S^{(n-1)} \tag{15}$$

when $V_{i(x=L_a)} < V_f$ oversteepening will be confined to the extent of the flow acceleration zone. Any advance of the

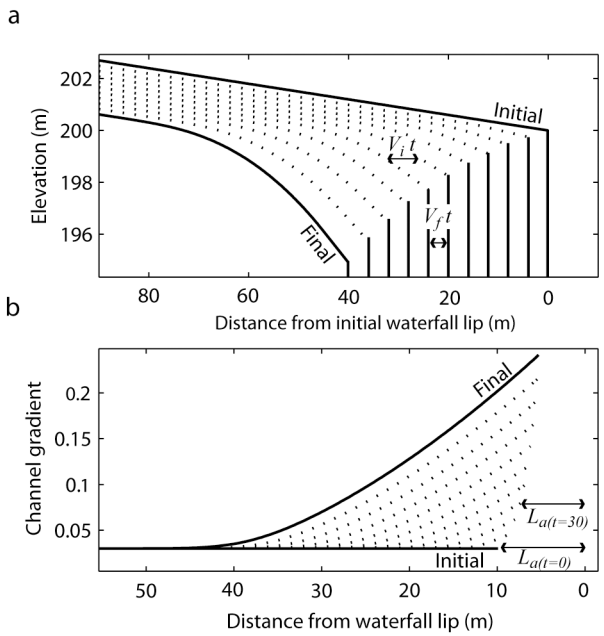

Figure 5. Results of numerical simulation of profile evolution above a waterfall whose face retreats upstream. Runtime is 100 kyr, n = 1, and V_f = 0.4 m/kyr. The calculated V_i value is 0.7 m/kyr and is independent of the distance from the lip, slope, and time. (a) Initial and final channel profile (solid) and profiles at 10 kyr intervals (dashed). Horizontal arrows delineate $V_f t$ and $V_i t$ for t = 10 kyr. Note that the waterfall face has retreated 40 m in 100 kyr while the oversteepening wave has retreated 80 m. The height of the waterfall lip decreases with time. (b) Initial and final channel gradient (solid) and channel gradients at 10 kyr intervals (dashed). Distance is measured from the waterfall lip which is a moving frame of reference. Note that L_{os} increases with time reaching 40 m after 100 kyr, $S_{(x < L_{os})}$ increases with time, and L_a decreases with time.

oversteepening wave of incision upstream from $x = L_a$, will eventually be matched by the retreat of the face. When $V_{i(x=L_a)} > V_f$ oversteepening will progressively extend upstream of the flow acceleration zone as depicted in Figure 5.

5. Influence of the Slope Exponent *n*

[19] Simulations where $V_{i(x=L_a,t=0)} > V_f$ were conducted using n values of 0.66, 1, and 1.2 (Figure 6). These values dictate that the upstream incision wave velocity (equation (15)) will decrease, remain constant, or increase as the channel slope increases, respectively.

[20] Higher value of n produced steeper oversteepened reaches (Figure 6a). In addition, the rate of increase of the slope adjacent to the lip ($dS_{(x=L_a)}/dt$) decreased with time for $n < 1$, increased with time for $n > 1$ and remained roughly constant for n = 1 (Figure 6b). These differences reflect the combined effects of the response of V_i to increasing slope for different values of n, and a greater erosion amplification for higher values of n. Since V_f approached V_i only for $n < 1$, it is only in this case that the slope at $x = L_a$ obtained steady state (Figure 6b). Gradients further upstream approached steady state in a time-transgressive manner: first at $x = L_a$ and only later at longer distances from the lip (Figure 6c).

6. Oversteepened Reach Length

[21] The length of the oversteepened reach (L_{os}) was time dependent in all runs and grew faster for higher values of n (Figure 6c). For n = 1, L_{os} is accurately predicted utilizing:

$$L_{os} = \left(V_{i(S=S_{initial})} - V_f\right)t + L_{a(t=0)} \tag{16}$$

For $n < 1$, L_{os} predicted using equation (16) was longer than its actual observed length because a significant part of the predicted oversteepened reach was only marginally oversteepened. This is expected because for $n < 1$ convexities diffuse as they are translated upstream [*Weissel and Seidl*, 1998; *Tucker and Whipple*, 2002]. The time dependency of L_{os} remained even when $S_{(x=L_a)}$ had already reached steady

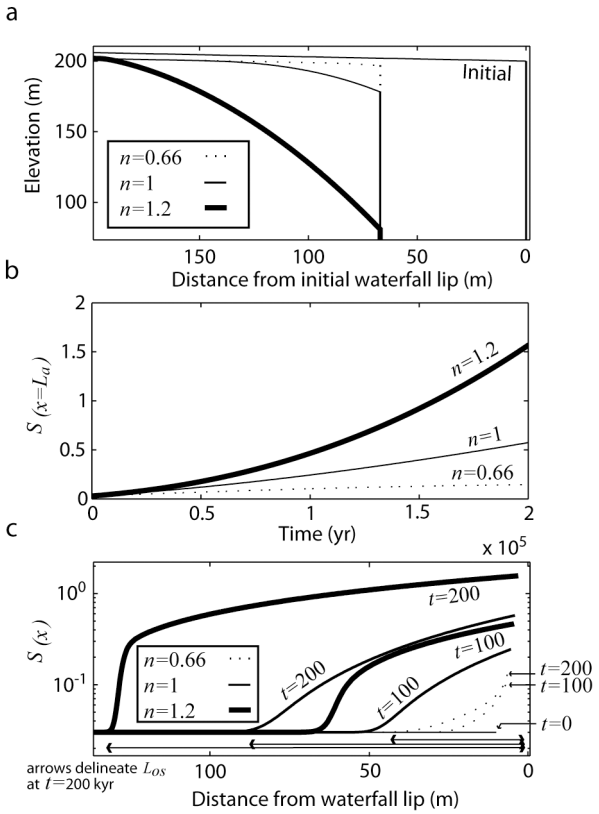

Figure 6. Model sensitivity to the parameter n. Run time is 200 kyr. V_f = 0.33 m/kyr. Initial incision rate away from the lip is set equal for all values of n. (a) Profile evolution. Note that the oversteepened reach is steeper when n is higher. (b) Channel gradient adjacent to the lip ($S_{(x=L_a)}$) as a function of time. Note that $S_{(x=L_a)}$ approaches a constant value for the n = 0.66 case. (c) Channel gradient depicted at t = 0, 100, 200 kyr. Distance is measured from the waterfall lip which is a moving frame of reference. Horizontal arrows illustrate the relative length of the oversteepened reach (L_{os}) for different n's at t = 200 kyr. Note that when n = 0.66, gradients near the lip hardly vary between the 100 kyr and 200 kyr runs while farther away from the lip they increase considerably.

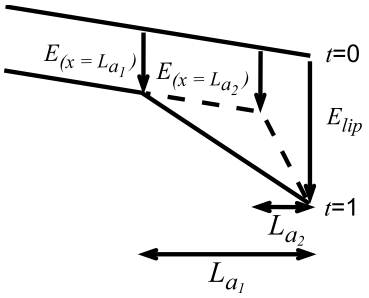

Figure 7. Model sensitivity to the initial length of the acceleration zone (L_a). When L_a is shorter, erosion amplification has a more pronounced influence on channel slope.

state since $V_{i(x=L_{os})}$ remained higher than V_f (Figure 6c). In other words, unlike the gradients in the lip vicinity there was no maximum limit for the length of the oversteepened reach. Note that this is only true for the short reaches modeled here where discharge does not decrease upstream. In the more general case, V_i can be expected to decrease as L_{os} grows in length and a steady state length of the oversteepened reach ought to be asymptotically approached.

[22] For the $n > 1$ case the model-observable L_{os} was significantly longer than the theoretical prediction given by equation (16). This occurs since when $n > 1$, $V_{i(x<L_{os})}$ increases as the slope increases, and the upstream edge of the oversteepened reach advances upstream at a rate which is faster than $V_{i(S=S_{initial})}$, migrates vertically, and gains elevation. These effects are amplified due to inevitable numerical diffusion even when the node spacing is very small.

7. Sensitivity to Roughness, Acceleration Length, and Episodic Face Retreat

[23] Higher values of the Manning roughness coefficient reduce the Froude number and in turn, increase the amplification of erosion at the lip. This higher amplification can lead to higher slopes adjacent to the lip. For rectangular, wide channels higher n_m will also increase erosion at $x = L_a$ because of the higher shear stress exerted on the bed. This is not necessarily true for narrow channels where higher roughness associated with wall drag may increase the average cross-sectional shear but decrease bed shear. It should be also stressed that the actual form of the amplification function (equation (11)), rather than just the value of the Froude number, may be roughness dependent.

[24] The higher the ratio between the length of the flow acceleration zone and the depth of the flow entering this zone (r, equation (13)), the lower is $S_{(x=L_a,t)}$ and thus the less pronounced is the oversteepened reach that develops. This follows because any increase in the elevation difference between the lip and x = L_a, during a given time interval, is spread over a longer distance when L_a is longer, and hence produces a lower increase in slope (Figure 7). The effect is more pronounced for higher values of n and V_i/V_f.

[25] Where waterfall retreat occurs episodically in discrete pulses, rather than quasi-continuously, it is possible that more than several thousand years will pass without significant translation of the waterfall face. Under such conditions the maximum length of the oversteepened reach may slightly exceed the length of the flow acceleration zone even if $V_{i(x=L_a)} < V_f$. For $n = 1$ this maximum length will be given by:

$$L_{os} = L_a + t_f V_i \tag{17}$$

where t_f is the time interval between failure episodes of the waterfall face.

8. Feasibility of Hydraulically Induced Oversteepening Along the Dead Sea Channels

[26] As mentioned earlier, hydraulically triggered oversteepening can extend upstream of the hydrodynamic flow acceleration zone only when fluvial incision at $x = L_a$ is sufficient to cause an upstream incision wave velocity, V_i (equation (14)) which outpaces the waterfall face retreat velocity, V_f. We chose Nahal Hever which drains into the Dead Sea 50 km southeast of Jerusalem (Figure 8a) to determine the ratio between these two velocities and thus to find out whether hydraulically induced oversteepening is feasible. The Hever waterfall is 130 m high and is located 6.5 km upstream from the outlet of the channel at the Dead Sea western tectonic escarpment (Figure 8b). The oversteepened reach above the waterfall is 850 m long (Figures 1 and 8b and Table 1).

[27] Incision wave velocity was quantified utilizing the cosmogenic isotope Cl-36. To measure V_i we sampled a horizontal dolomitic limestone strath which still preserves fluvially sculptured bed forms and extends 180 m upstream from Hever waterfall (Figure 8c). The samples were a few centimeters thick and were picked from elevated bed forms upon the strath where minor post strath formation weathering has occurred. The distance between each sample and the lip exceeds L_a (85–180 m; $L_a \cong 15$ m; $L_{os} = 850$ m). Cl-36 accumulation in samples collected from the strath was modeled as a two stage scenario. In the first stage the rock mass of each sample is taken to be at the level of the channel bed with a Cl-36 concentration dictated by the background channel incision rate. Following incision of the channel below the strath surface it is assumed that erosion of the surface practically ceases. The concentration of Cl-36 added to each sample during this second stage is therefore a function of the time since the strath was abandoned. To estimate the Cl-36 acquired during the first stage we sampled the bed of the current active channel upstream of the strath (H4 in Figure 8c; see footnotes of Table 2 for details). By doing so we assume that incision rate upstream of the strath is representative and did not vary significantly over time.

[28] All the samples were prepared at the University of Washington cosmogenic isotope lab using procedures described by *Stone et al.* [1996, 1998] and were measured using the 14-UD Pelletron accelerator mass spectrometer (AMS) of the Australian National University [*Fifield et al.*, 1994]. The main stages of sample preparation included grinding and sieving each sample to derive a 125–250 micron fraction, leaching and dissolving the leached sample using nitric acid, removing sulfur (and the isobar S-36) from the solution and precipitating AgCl for AMS analysis. Chloride concentrations were determined using isotope

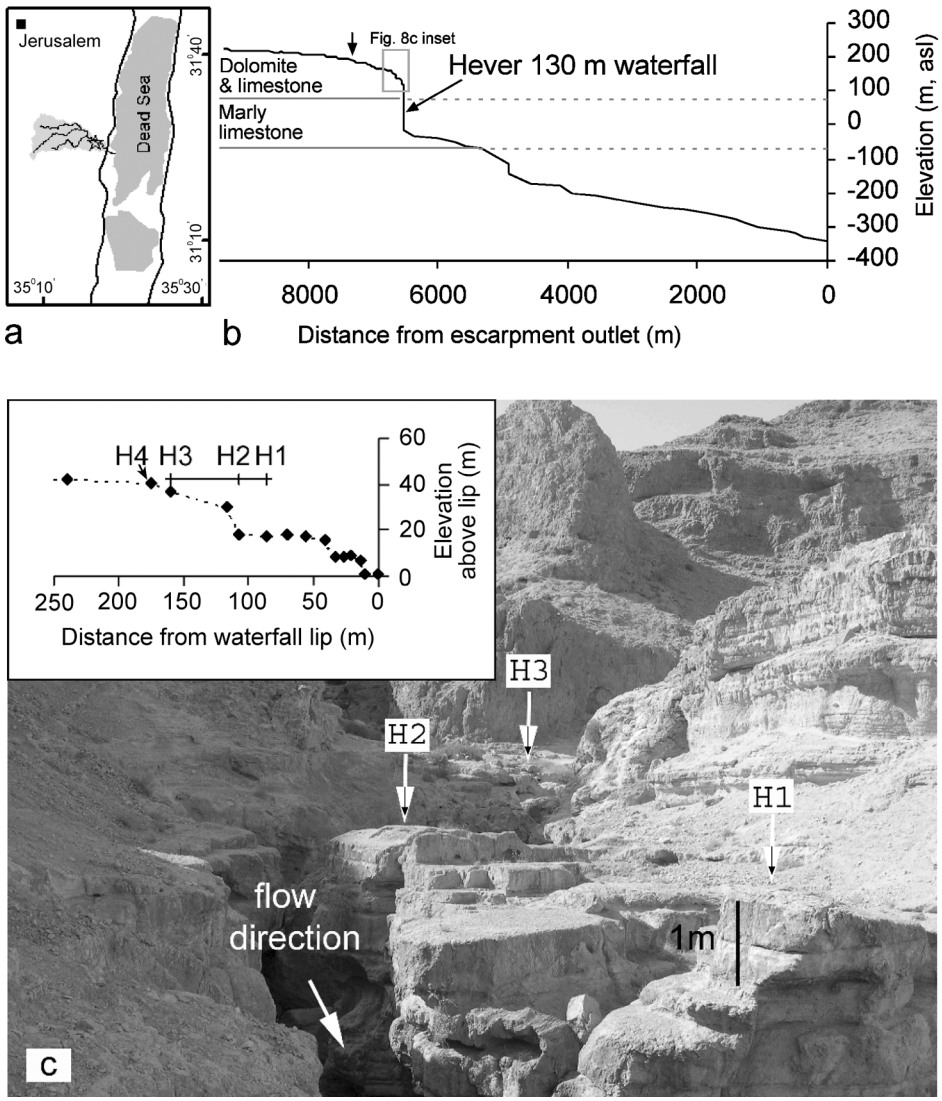

Figure 8. Nahal Hever case study. (a) Location map. The base of the Dead Sea eastern and western tectonic escarpments are marked as black lines. Hever waterfall is marked by a star symbol. (b) Longitudinal profile of Nahal Hever from its outlet at the Dead Sea western escarpment to ~3 km upstream of Hever waterfall. Distance and elevation data below the waterfall were extracted from 1:50,000 map, whereas above the waterfall the reach was surveyed using a laser range finder and a hand level. Arrow delineates the upstream end of the oversteepened reach above the waterfall. (c) The strath from where samples H1–H3 were collected. Channel bed is located at depths of 0–40 m below the strath. Note the fluvially sculpted bed forms of samples H1–H3. Inset provides a zoom-in on the channel profile (dashed line with solid diamonds) and the strath (solid line) upstream of the waterfall with Cl-36 sampling locations.

dilution with Cl-37 on a split from the solution of each sample.

[29] The calculated exposure ages for the Hever strath samples are 45.4 ± 3.4, 33.4 ± 2.5 and 3.1 ± 1.0 kyr for H1, H2 and H3, respectively (Figure 8c, Table 2). As expected they indicate that the strath surface is time transgressive, i.e., the farther upstream the more recently the channel has incised below the surface. Dividing the distance between each two samples (21, 53 and 74 m for H1–H2, H2–H3 and H1–H3, respectively) by the difference in their exposure ages yields the average V_i during the relevant time span. These average velocities are 1.7 ± 0.6, 1.8 ± 0.2 and 1.8 ± 0.2 m/kyr for H1–H2, H2–H3 and H1–H3, respectively. The latter rate represents the average V_i for a ~42 kyr period.

[30] Average long-term face retreat velocities for Hever waterfall were estimated on the basis of the distance of the waterfall from the base of the Dead Sea western tectonic escarpment and a 4–8 Myr exhumation age for the lithologic transition (from resistant dolomite and limestone to weak marly limestone (Figure 8b)), which is responsible for the waterfall generation [*Haviv et al.*, 2003]. This exhumation age is an estimate based on K-Ar ages of basalt flows along the Dead Sea eastern escarpment [*Steinitz and Bartov*,

Table 2. Cl-36 Results

Sample	Geomorphic Location, Figure 8	Cl-36 Concentration, 10^5 atoms/g	Production Rate[a] of Cl-36, atoms/g/yr	Inherited[b] Cl-36 Concentration, 10^5 atoms/g	Exposure Age[c], kyr
H1	Strath	8.23 ± 0.42	16.06 ± 0.57	1.44 ± 0.17	45.4 ± 3.4
H2	Strath	7.69 ± 0.38	18.92 ± 0.68	1.73 ± 0.22	33.4 ± 2.5
H3	Strath	2.00 ± 0.16	16.71 ± 0.59	1.48 ± 0.19	3.1 ± 1.0
H4	Channel bed	1.05 ± 0.14	10.92 ± 0.45	not relevant	not relevant

[a]Production rates were calculated using a sea level, high-latitude value of 54 atoms/gCa/yr for total production from Ca, partitioned between spallation (48.8 ± 3.4 atoms/gCa/yr) and muon capture reactions (5.2 ± 1.2 atoms/gCa/yr) as described by *Stone et al.* [1996, 1998]. The samples do not contain significant amounts of K, Ti or Fe. Production rates were scaled to altitude and latitude as described by *Lal* [1991] and corrected for thickness and exposure geometry using standard methods. Production rates by thermal and epithermal neutron capture were calculated using the method of *Phillips et al.* [2001].

[b]Inherited Cl-36 concentrations at the surface of the strath, for each of the sampling locations, were calculated utilizing a channel incision rate of 127 ± 21 m/Myr derived on the basis of H4. These inherited concentrations were calculated, rather than taken as identical to the measured concentration of H4, in order to account for differences in the chemistry of the samples (mainly Ca concentration) and shielding geometry.

[c]Exposure ages since the strath was cut at each sampling position were calculated utilizing: $N = \frac{P}{\lambda}(1 - e^{-\lambda t}) + N_i e^{-\lambda t}$ [*Lal*, 1991] where N is the measured Cl-36 concentration, P is production rate, λ is Cl-36 decay constant and N_i is the inherited Cl-36 concentration at the surface of the starth.

1992], assuming the western and eastern escarpments evolved simultaneously. Old basalt flows whose age is 6–8 Myr are restricted to a low-relief plateau which terminates at the eastern escarpment [*Steinitz and Bartov*, 1992]. These basalt flows do not extend into the valleys and at least in one setting appear to have flowed across what is currently a deep canyon. Unlike the old basalts, younger 0.5–4 Myr basalts can be found at relatively low elevations within deep canyons indicating that more than half of the relief of the eastern escarpment is older than 4 Myr and younger than 6 Myr. If half or more of the western escarpment relief evolved during this same period the lithologic transition which is responsible for the generation of Hever waterfall (Figure 8b) was exhumed earlier than 4 Myr ago.

[31] The average long-term V_f for Hever waterfall, calculated using the above procedure, is 0.8–1.6 m/kyr and is probably lower than the cosmogenically derived V_i (1.7 ± 0.6, 1.8 ± 0.2 and 1.8 ± 0.2 m/kyr). Under the following two assumptions the results indicate that waterfall-related oversteepening has extended beyond the flow acceleration zone (L_a) and has created a long-oversteepened reach: (1) Measured V_i rates can be taken to represent a much longer period than they actually do (millions of years instead of ~50 kyr). (2) V_i closer to the lip at $x = L_a$ is similar to the measured values.

9. Discussion

[32] Flow acceleration and erosion amplification at a waterfall lip result from low pressures at the lip cross section. Therefore hydraulically induced oversteepening above a waterfall should probably be more dominant where the flow cross section at the lip is in contact with the air around its entire perimeter. Such conditions, where the falling jet is not confined by sidewalls, are common where waterfalls consist of resistant caprock and erodible footrock, since the erodible rocks dictate milder hillslopes and hence a wider valley downstream of the waterfall. Where the falling jet is confined by walls and the face is inclined, rather then vertical, oversteepening should be less pronounced. Nevertheless, *Gardner* [1983, his Figure 8] has demonstrated in a flume study that flow velocity and shear stress increase even where water approaches a transition from mild to steep slope and channel width across the transition is almost fixed. Unlike oversteepened reaches above vertical waterfalls, in the mild steep transition case the length of the oversteepened reach should be confined to the acceleration zone (L_a) unless incision wave velocity decreases with increasing slope. When this is not the case the original break in slope will retreat at a rate faster than or equal to that of the oversteepening wave.

[33] The existence of oversteepened reaches above waterfalls such as those of the Blue Mountains, the Dead Sea western escarpment and Niagara Falls is not enough to prove that these reaches were formed because of the waterfalls at their terminus. Such reaches could also reflect rock strength properties, a migrating incision signal or exhumation of a resistant flat-lying formation under conditions where E/S decreases as slope increases (for example when $n < 1$, see Figure 8 *Tucker and Whipple* [2002]). Regardless of these other plausible triggers, flow acceleration near a freefall and the erosion amplification associated with it are sufficient to produce a long convex reach upstream of a waterfall, provided $V_{i(x=L_a)} > V_f$. As demonstrated for Hever waterfall, quantifying these two variables in the field can help decipher the origin of an oversteepened reach.

[34] Factors which act to alter the ratio between V_f and V_i will influence the lengthening or shortening rate of the oversteepened reach. The ratio between these two velocities may be discharge dependent and could thus vary as a waterfall retreats upstream and drainage area decreases regardless of any external perturbation. Utilizing equation (15) to express $V_{i(x=L_a)}$ and assuming V_f can be written as a power law function of discharge [*Haviv et al.*, 2003; *Hayakawa and Matsukura*, 2003; *Enzel et al.*, 2005; *Crosby and Whipple*, 2006] this ratio can be expressed as:

$$\frac{V_f}{V_i} = \frac{K_f}{KS^{(n-1)}} A^{(m_f - m)} \tag{18}$$

where K_f and m_f are face erodibility and face drainage area exponent, respectively. It is therefore possible that even where climatic, lithologic and tectonic conditions are steady and uniform a waterfall which lacked an oversteepened reach may eventually develop one (e.g., when $n = 1$, $m_f > m$ and $K_f < K$) and visa versa (e.g., when $n = 1$, $m_f < m$ and $K_f > K$). We speculate that the latter conditions should be more common in nature since mass failure mechanisms responsible for lateral erosion of vertical faces should

probably be less sensitive to discharge ($m_f < m$) than normal fluvial incision. If so, oversteepened reaches should be shorter and less abundant at small drainages (compared to large drainage areas) and where waterfalls are located not far from divides.

[35] A ''delayed'' development of oversteepened reaches can occur where earthquake-induced ground accelerations have a significant enhancing influence on waterfall face retreat velocity. Under such a scenario oversteepened reaches may start to evolve when the prevailing tectonic rates decrease or at a certain distance from a tectonic escarpment.

[36] Some interesting preliminary predictions arise if other erosion laws, rather than the stream power erosion law, are used in conjunction with our erosion amplification function (equation (11)). The *Sklar and Dietrich* [1998, 2004] bed load saltation erosion law is expected to drive the gradients in the vicinity of the waterfall toward steady state in a similar manner to the $n < 1$ case. Such a behavior is expected since as the slope increases beyond a certain threshold, erosion rates predicted by the bed load saltation model actually decrease. This decrease is driven by a decrease in the number of particle impacts per unit channel length as particle hop length increases.

[37] When *Whipple and Tucker*'s [2002] linear sediment-flux-dependent erosion law is used (the so-called 'linear decline' model), V_i will increase as the slope rises even when $n = 1$. In addition when $n < 1$ and the slope above the waterfall rises, V_i will decrease less than it does in the standard detachment limited model. The 'linear decline' model assumes $E = f(q_s)KA^mS^n$, where $f(q_s)$ is erodibility scaling factor for sediment loading given by: $f(q_s) = 1 - Q_s/Q_c$, Q_s is bed load sediment discharge and Q_c is bed load sediment transport capacity. The above mentioned effects of the 'linear decline' model reflect a decrease in channel bed armoring as the transport capacity increases and will promote more pronounced oversteepened reaches.

10. Conclusions

[38] We developed a model of the expected erosion amplification at a waterfall lip and examined the interaction between erosion at the lip, retreat of the waterfall face (Figure 2a), and profile evolution upstream of the waterfall. This model can explain the common occurrence of oversteepened reaches above vertical waterfalls. Although other factors can create oversteepened reaches they could also be the sole result of freefall-induced flow acceleration.

[39] Erosion amplification at a waterfall lip is expected to be a decreasing function of the Froude number (Fr) at the upper end of the acceleration zone and an increasing function of the slope exponent n. For $Fr \approx 1$ erosion at the lip could be 2–5 times higher than erosion at the upstream end of the flow acceleration zone. Erosion amplification is expected even when the flow approaching the waterfall is highly supercritical. This amplified erosion can trigger the formation of an oversteepened reach whose length is significantly larger than the flow acceleration zone. For this to happen, incision wave velocity at the upper end of the acceleration zone should be larger than the waterfall face retreat velocity.

[40] Oversteepened reaches are expected to be more pronounced where incision wave velocity increases as the slope increases. Interestingly, where incision wave velocity decreases as the slope increases gradients near the lip will eventually approach steady state.

[41] Using the cosmogenic isotope Cl-36 we demonstrate that incision wave velocity upstream of a waterfall at the Dead Sea western escarpment is probably high enough for freefall-induced oversteepening to be feasible.

Notation

A	upstream drainage area, [L^2].
A_{c_lip}	flow cross-sectional area at a waterfall lip [L^2].
$A_{c(x=L_a)}$	flow cross-sectional area at a distance L_a from a waterfall lip [L^2].
a	shear stress exponent, detachment-limited erosion rule, dimensionless.
E	vertical erosion rate [$L\ T^{-1}$].
E_{lip}	vertical erosion rate at the lip of a waterfall [$L\ T^{-1}$].
$E_{(x=L_a)}$	vertical erosion rate at a distance L_a from a waterfall lip [$L\ T^{-1}$].
$f(q_s)$	erodibility scaling factor for sediment loading, dimensionless.
Fr	flow Froude number, dimensionless.
$Fr_{(x=L_a)}$	flow Froude number at a distance L_a from a waterfall lip, dimensionless.
g	gravitational acceleration [$L\ T^{-2}$].
h_{lip}	flow depth at a waterfall lip [L].
$h_{(x=L_a)}$	flow depth at a distance L_a from a waterfall lip [L].
K	coefficient of erosion [$L^{1-2m}\ T^{-1}$].
K_f	coefficient of erosion, waterfall face lateral erosion rule [$L^{1-2m}\ T^{-1}$].
L_a	length of flow acceleration zone upstream of a waterfall [L].
L_{os}	length of oversteepened reach upstream of a waterfall [L].
m	area exponent, detachment-limited erosion rule, dimensionless.
m_f	area exponent, vertical face lateral erosion rule, dimensionless.
m_w	mass of water passing a given cross section during time Δt [M].
n	slope exponent, detachment-limited erosion rule, dimensionless.
n_m	Manning roughness coefficient, dimensionless.
P_{lip}	average hydraulic pressure at flow cross section at a waterfall lip [$M\ T^{-2}\ L^{-1}$].
$P_{(x=L_a)}$	average hydraulic pressure at flow cross section at a distance L_a from a waterfall lip [$M\ T^{-2}\ L^{-1}$].
Q	discharge [$L^3\ T^{-1}$].
Q_c	bed load sediment transport capacity [$L^3\ T^{-1}$].
Q_s	bed load sediment flux [$L^3\ T^{-1}$].
q	discharge per unit width [$L^2\ T^{-1}$].
r	ratio between L_a and flow depth at L_a, dimensionless.
S	channel bed gradient, dimensionless.
t	time [T].
t_f	time interval between failure events at a waterfall face [T].
V_i	incision wave velocity [$L\ T^{-1}$].
V_f	waterfall face retreat velocity [$L\ T^{-1}$].

V_{lip} average flow velocity parallel to the channel at a waterfall lip [L T^{-1}].
$V_{(x=L_a)}$ average flow velocity at distance L_a from a waterfall lip [L T^{-1}].
w channel width [L].
x distance from a waterfall lip [L].
α channel gradient measured in degrees.
ρ water density [M L^{-3}].
τ_{lip} average boundary shear stress at a waterfall lip [M T^{-2} L^{-1}].
$\tau_{(x=L_a)}$ average boundary shear stress at a distance L_a from a waterfall lip [M T^{-2} L^{-1}].

[42] **Acknowledgments.** This research was funded by grant 2002-159 from the United States-Israel Bi-National Science Foundation. Additional support was provided by Asher Schick's Student Research Award 2004. We thank the remarkable staff of Ein Gedi field school for their hospitality and assistance in the field. We also thank Uri Ryb, Eldad Levi, Boaz Tatarsky, and Yehouda Shalem for helping in the field. We acknowledge the helpful comments raised by reviewers Alex Densmore, Leonard Sklar, and Robert Anderson.

References

Crosby, B., and K. X. Whipple (2006), Knickpoint initiation and distribution within fluvial networks: 236 waterfalls in the Waipaoa River, North Island, New Zealand, *Geomorphology*, in press.

Delleur, J. W., J. C. I. Dooge, K. W. Gent, and E. M. Laursen (1956), Influence of slope and roughness on the free overfall, *J. Hydraul. Div. Am. Soc. Civ. Eng.*, *82*, 30–35.

Enzel, Y., I. Haviv, E. Zilberman, K. X. Whipple, J. Stone, A. Matmon, and L. K. Fifield (2005), Waterfall retreat rates along the Dead Sea western tectonic escarpment, *Eos Trans. AGU*, *86*(52), Fall Meet. Suppl., Abstract H53D-0518.

Fifield, L. K., G. L. Stone, and T. R. Ophel (1994), The ANU AMS system and research program, *Nucl. Instrum. Methods Phys. Res., Sect. B*, *92*, 85–89.

Gardner, T. W. (1983), Experimental study of knickpoint and longitudinal profile evolution in cohesive, homogeneous material, *Geol. Soc. Am. Bull.*, *94*, 664–672.

Hager, W. H. (1983), Hydraulics of the plane free overfall, *J. Hydraul. Eng.*, *109*, 1683–1697.

Hager, W. H. (1984), Hydraulics of the plane free overfall: Errata, *J. Hydraul. Eng.*, *110*, 1683–1697.

Hancock, G. S., R. S. Anderson, and K. X. Whipple (1998), Beyond power, bedrock incision process and form, in *Rivers Over Rock: Fluvial Processes in Bedrock Channels*, *Geophys. Monogr. Ser.*, vol. 107, edited by K. J. Tinkler and E. E. Wohl, pp. 35–60, AGU, Washington, D. C.

Haviv, I., Y. Enzel, E. Zilberman, K. X. Whipple, J. Stone, A. Matmon, and K. L. Fifield (2003), Knickpoint retreat and drawdown reach evolution along the arid escarpments of the Dead Sea Basin, abstract, *Geol. Soc. Am. Abstr. Programs*, *35*, 333.

Hayakawa, Y., and Y. Matsukura (2003), Recession rates of waterfalls in Boso Peninsula, Japan, and a predictive equation, *Earth Surf. Processes Landforms*, *28*, 675–684.

Hayakawa, Y. S., S. Yokoyama, and Y. Matsukura (2005), Rates of waterfall recession in welded ignimbrites of Aso volcanoes in central Kyushu, Japan, abstract 508, paper presented at the 6th International Conference on Geomorphology, Intl. Assoc. of Geomorphol., Zaragoza, Spain, September 7–11.

Henderson, F. M. (1966), *Open Channel Flow*, Macmillan, New York.

Holland, W. N. (1974), Origin and development of hanging valleys in the Blue Mountains, New South Wales, Ph.D. dissertation, 364 pp., Sydney Univ., Australia.

Howard, A. D., and G. Kerby (1983), Channel changes in badlands, *Geol. Soc. Am. Bull.*, *30*, 2261–2285.

Johnson, J. P., and K. X. Whipple (2004), Experimental bedrock channel incision: Scaling, sculpture and sediment transport, *Eos Trans. AGU*, *85*(47), Fall Meet. Suppl., Abstract H41G-07.

Lal, D. (1991), Cosmic ray labeling of erosion surfaces: In situ nuclide production rates and erosion models, *Earth Planet. Sci. Lett.*, *104*, 424–439.

Philbrick, S. S. (1970), Horizontal configuration and the rate of erosion of Niagara Falls, *Geol. Soc. Am. Bull.*, *81*, 3723–3732.

Philbrick, S. S. (1974), What future for the Niagara Falls?, *Geol. Soc. Am. Bull.*, *85*, 91–98.

Phillips, F. M., W. D. Stone, and J. T. Fabryka-Martin (2001), An improved approach to calculating low energy cosmic-ray neutron fluxes near the land/atmosphere interface, *Chem. Geol.*, *175*, 689–701.

Rajaratnam, M., and D. Muralidhar (1968a), Characteristics of the rectangular free overfall, *J. Hydraul. Res.*, *3*, 233–258.

Rajaratnam, M., and D. Muralidhar (1968b), The rectangular free overfall, *J. Hydraul. Div. Am. Soc. Eng.*, *94*, 849–850.

Rajaratnam, M., D. Muralidhar, and S. Beltaos (1976), Roughness effects on rectangular free overfall, *J. Hydraul. Div. Am. Soc. Eng.*, *102*, 599–614.

Rosenbloom, N. A., and R. S. Anderson (1994), Hillslope and channel evolution in marine terraced landscape, Santa Cruz, California, *J. Geophys. Res.*, *99*(B7), 14,013–14,029.

Rouse, H. (1936), Discharge characteristics of the free overfall, *Civ. Eng.*, *6*, 257–260.

Rouse, H. (1937), Pressure distribution and acceleration at the free overfall, *Civ. Eng.*, *7*, 518.

Rouse, H. (1943), Discussion to "Energy loss at base of a Free overfall" by W. L. Moore, *Trans. Am. Soc. Civ. Eng.*, *108*, 1383–1387.

Seidl, M. A., and W. E. Dietrich (1992), The problem of channel erosion into bedrock, in *Functional Geomorphology*, edited by K. H. Schmidt and J. de Ploey, *Catena Suppl.*, *23*, 101–124.

Sklar, L. S., and W. E. Dietrich (1998), River longitudinal profiles and bedrock incision models: Stream power and the influence of sediment supply, in *Rivers Over Rock: Fluvial Processes in Bedrock Channels*, *Geophys. Monogr. Ser.*, vol. 107, edited by K. J. Tinkler and E. E. Wohl, pp. 237–260, AGU, Washington, D. C.

Sklar, L. S., and W. E. Dietrich (2004), A mechanistic model for river incision into bedrock by saltating bed load, *Water Resour. Res.*, *40*, W06301, doi:10.1029/2003WR002496.

Sklar, L. S., J. D. Stock, J. J. Roering, J. W. Kirchner, and W. E. Dietrich (2005), Rapid evolution of fault scarp knickpoints following September 1999 Chi-Chi earthquake in West-Central Taiwan, abstract 507, paper presented at 6th International Conference on Geomorphology, Intl. Assoc. of Geomorphol., Zaragoza, Spain, September 7–11.

Stein, O. R., and P. Y. Julien (1993), Criterion delineating the mode of headcut migration, *J. Hydraul. Eng.*, *119*, 37–50.

Steinitz, G., and Y. Bartov (1992), The Miocene-Pleistocene history of the Dead Sea segment of the rift in light of K-Ar ages of basalts, *Isr. J. Earth Sci.*, *40*, 199–208.

Stock, J. D., and D. R. Montgomery (1999), Geological constraints on bedrock river incision using stream power law, *J. Geophys. Res.*, *104*(B3), 4983–4993.

Stone, J. O., G. L. Allan, L. K. Fifield, and R. G. Cresswell (1996), Cosmogenic Cl-36 from calcium spallation, *Geochim. Cosmochim. Acta*, *60*, 679–692.

Stone, J. O., J. M. Evans, L. K. Fifield, G. L. Allan, and R. G. Cresswell (1998), Cosmogenic Cl-36 production in calcite by muons, *Geochim. Cosmochim. Acta*, *62*, 433–454.

Tucker, G. E., and K. X. Whipple (2002), Topographic outcomes predicted by stream erosion models: Sensitivity analysis and intermodel comparison, *J. Geophys. Res.*, *107*(B9), 2179, doi:10.1029/2001JB000162.

Weissel, J. K., and M. A. Seidl (1998), Inland propagation of erosional escarpments and river profile evolution across the southeast Australian passive continental margin, in *Rivers Over Rock: Fluvial Processes in Bedrock Channels*, *Geophys. Monogr. Ser.*, vol. 107, edited by K. J. Tinkler and E. E. Wohl, pp. 189–206, AGU, Washington, D. C.

Whipple, K. X., and G. E. Tucker (1999), Dynamics of the stream-power river incision model: Implications for height of mountain ranges, landscape response timescales, and research needs, *J. Geophys. Res.*, *104*(B8), 17,661–17,674.

Whipple, K. X., and G. E. Tucker (2002), Implications of sediment-flux-dependent river incision models for landscape evolution, *J. Geophys. Res.*, *107*(B2), 2039, doi:10.1029/2000JB000044.

Whipple, K. X., G. S. Hancock, and R. S. Anderson (2000), River incision into bedrock: Mechanics and relative efficacy of plucking, abrasion, and cavitation, *Geol. Soc. Am. Bull.*, *112*, 490–503.

Y. Enzel, I. Haviv, and A. Matmon, Institute of Earth Sciences, The Hebrew University of Jerusalem, Givat Ram, Jerusalem, 91904, Israel. (haviv@vms.huji.ac.il)

L. K. Fifield, Department of Nuclear Physics, Australian National University, Canberra, ACT-0200, Australia.

J. Stone, Quaternary Research Center, University of Washington, 19 Johnson Hall, Box 351360, Seattle, WA 98195, USA.

K. X. Whipple, Earth, Atmospheric and Planetary Sciences, Massachusetts Institute of Technology, Cambridge, MA 02139, USA.

E. Zilberman, Geological Survey of Israel, 30 Malkhe Israel, Jerusalem, 95501, Israel.